Progress In Electromagnetics Research M, Vol. 101, 59–68, 2021

Broadband and High-Aperture Efficiency Fabry-Perot Antenna with Low RCS Based on Nonuniform Metamaterial Superstrate

Hui-Fen Huang* **and Qi-Sheng Fan**

Abstract—Due to the nonuniform Electromagnetic (EM) field distribution over the superstrate, a Fabry-Perot Resonant Antenna is normally with high directivity but relatively low aperture efficiency when its aperture size is electrically large. In this paper, a Fabry-Perot resonator cavity antenna (FPCA) with a nonuniform metamaterial superstrate is proposed. The nonuniform metamaterial superstrate is a nonuniform double-sided printed dielectric, in which the upper surface is used for wideband RCS reduction, and the bottom surface is the nonuniform partially reflective surface (PRS) of FPRA for wideband and high aperture efficiency performances. Wideband RCS reduction is realized by designing the phase differences 90° in turn among three adjacent frequency-selective surfaces. The wideband 3 dB gain bandwidth and high aperture efficiency performances are obtained by designing the PRS with a positive reflection phase gradient vs frequency and a negative transverse-reflection magnitude gradient, respectively. The measured results show that the gain of the proposed antenna is 11.5 dBi greater than that of the primary source antenna with a peak value 15.5 dBi at 9.2 GHz. The aperture efficiency is 73.3%. The 3-dB gain bandwidth is from 8.75 to 11.47 GHz (26.9%), and the RCS reduction can be obtained effectively from 8.2 to 20 GHz (83.7%).

1. INTRODUCTION

Fabry-Perot cavity antennas (FPCAs) have recently attracted broad interests from research in both physics and engineering communities, due to their interesting features of high gain and planar configuration [1]. FPCA usually consists of a primary radiator embedded inside a cavity formed by locating a nearly half a wavelength metasurface above a metal ground plate. Recently, radar cross-section (RCS) reduction has received extensive attentions. As a special scatterer for communication and radar systems, antennas on the stealth platforms make great contribution to the overall RCS [2]. The idea of achieving a high-gain and low-RCS Fabry-Perot antenna was first proposed in [3]. Many low-RCS Fabry-Perot antennas have been proposed [3–5]. In these Fabry-Perot resonance structures, the superstrate of the FPCA is double-sided printed dielectric; the upper surface is for RCS reduction, and the bottom surface is PRS of FPRA. However, all of these F-P antennas do not realize wideband gain bandwidth. Hence, many attempts have been made to overcome the shortcoming of such antennas. A superstrate, which consists of multilayer same or different dielectrics, is employed to create multiple resonances [6]. However, the antenna profile was increased, and the mechanical stability of the antenna was disturbed. Novel all-dielectric PRS was studied to enhance the gain bandwidth obviously, which is composed of different dielectric materials and possesses the property of effective gradient permittivity in the transverse direction [7, 8]. However, the manufacturing process was a little complex. In addition, frequency selection surfaces (FSSs) have also been proposed as a class of wideband PRS [9]. To realize a

Received 9 December 2020, Accepted 7 February 2021, Scheduled 18 February 2021
* Corresponding author: Hui-Fen Huang (huanghf@scut.edu.cn).
The authors are with the School of Electronic and Information Engineering, South China University of Technology, Guangzhou, China.

wideband 3 dB gain bandwidth, the reflection phase of the PRS layer was designed to possess a positive slope vs frequency in a wide frequency band [10–13].

Meanwhile, research on achieving high aperture efficiency has also been conducted. The electric field magnitude decreases from inner to outer areas throughout the cavity for conventional FPCA, which bring out poor aperture efficiency and worse peak gain. This led to the assumption that an unconventional PRS with negative transverse-reflection magnitude gradient to realizes the equal amplitude and cophasal distributions respectively for its aperture electromagnetic field, and thus enhance its aperture efficiency [10, 14]. Although these approaches obtain good wideband gain enhancement performance and high aperture efficiency, they cannot achieve broadband RCS reduction. It may be a challenge to realize wideband 3-dB gain bandwidth and RCS reduction.

In this paper, wideband and high aperture efficiency techniques are utilized to realize an FPCA having multiple advantages of wideband $|S_{11}|$ bandwidth, high gain, low RCS, and high aperture efficiency. Wideband 3 dB gain bandwidth and high aperture efficiency are realized by utilizing a nonuniform PRS (NPRS) which has both positive reflection phase gradient and negative transverse-reflection magnitude properties. The wideband RCS reduction is realized by designing the phase differences 90° in turn among four adjacent frequency-selective surfaces. The rest of the paper is organized as follows. Section 2 shows the theory and antenna design. The antenna performance analysis is in Section 3. Experimental results are provided in Section 4, and Section 5 is conclusion.

2. THEORY AND ANTENNA DESIGN

2.1. Design Theory

As we all know, by combining two different kinds of artificial magnetic conductors with $180° \pm 30°$ phase difference in a checkerboard arrangement, the reflected waves will produce destructive interference under a normal incident plane wave for reducing the monostatic RCS in the normal direction [15, 16]. For the case of more kinds of artificial magnetic conductors, the RCS reduction may be a challenge. So in order to achieve a wideband RCS reduction, four different kinds of artificial magnetic conductors are employed, whose reflected phase differences between adjacent units are nearly 90° in turn, and the reflected waves will be canceled with each other, thus the monostatic RCS can be reduced by at least 6 dB [17]. In this paper, four kinds of frequency-selective surfaces with adjacent reflection phase difference 90° in turn are used to design the low RCS reduction surface.

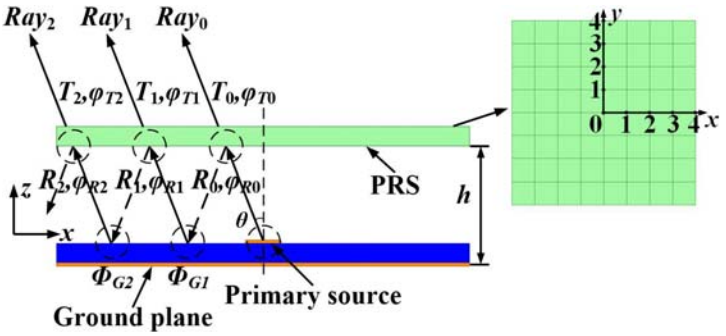

Figure 1. The working principle diagram of FPCA.

The working principle diagram of FPCA is shown in Fig. 1. The relationship between the frequency resonance of an FP resonator antenna and the reflection phase can be defined as

$$\varphi_{\mathrm{PRS}} = \frac{4\pi h}{c} f - \varphi_G + 2n\pi, \quad n = 0, 1, 2... \tag{1}$$

where φ_{PRS} and φ_G represent the reflection phases of the PRS layer and ground plane, respectively, and h is the height of the FP cavity. The phase difference between any two adjacent rays, Ray_{N+1} and

Ray_N, is

$$\phi_{N+1} = \phi_{RN} + \phi_{G(N+1)} + \phi_{T(N+1)} - \phi_{TN} - \frac{K \cdot 2h}{\cos\theta} + K \cdot 2h \tan\theta \sin\theta \tag{2}$$

where K is the wave number, and θ is marked in Fig. 1. The "in phase" condition between any two adjacent rays, Ray_{N+1} and Ray_N, for any N satisfies:

$$\phi_{N+1} = 2n\pi \tag{3}$$

where n is an integer. The relation between the directivity (D) of the FP resonator antenna and the reflection magnitude ($|\Gamma|$) of the PRS layer is as follows.

$$D = 10 \log \frac{1 + |\Gamma|}{1 - |\Gamma|} \tag{4}$$

From Eqs. (1) and (4), the reflection phase increases when frequency goes up, and larger reflection magnitude leads to higher directivity. Hence, to achieve a broadband high-gain FP resonator antenna, the reflection phase of the PRS layer on the bottom surface of the superstrate should be designed to have a positive gradient, and the reflection magnitude should not be small in the desired frequency band [18]. In addition, an unconventional PRS with negative transverse-reflection magnitude gradient realizes the equal amplitude and cophasal distributions respectively for its aperture electromagnetic field, and thus enhances its aperture efficiency. The field amplitude on the FPRA aperture against the number of reflections N (N is noted in Fig. 1) can be expressed as [19]:

$$|E_N| = E_P \cdot |\Gamma|^{N-1} \sqrt{1 - |\Gamma|^2} \tag{5}$$

where E_P represents the field of the feed antenna, and $|\Gamma|$ is the reflection magnitude of the superstrate. The amplitude of E_N decreases exponentially with the increase in the number of reflections. This means that a nonuniform EM field amplitude distribution forms over the FPRA's aperture. According to Eq. (5), to produce a uniform field amplitude distribution, the reflection magnitude of the superstrate should be nonuniform and decrease with the increase in the number N of reflections, thereby providing compensation for the exponentially decreased amplitude. Therefore, to obtain FPCA with wideband high aperture efficiency and high gain, the PRS is designed to satisfy following conditions: (a) Negative transverse-reflection magnitude gradient; (b) a positive phase gradient vs frequency; (c) the reflection magnitude should not be small; (d) the rays are in phase.

2.2. FPCA Superstrate Structure Analysis

Figures 2(a), (b), (c), (d) are the schematic diagram, overall, top and bottom views of the superstrate, respectively. The superstrate is made in a F4B dielectric substrate with the thickness of 3 mm and relative permittivity of 2.65. The superstrate consists of four kinds of FSS units with different sizes marked in FSS (1–4) as in Fig. 2(b), and these FSS units are arranged in a configuration of four concentric square frames, respectively. Such a design can cover a larger area with fewer parameters. The upper surface of the superstrate is for RCS reduction, and the bottom surface is nonuniform PRS (NPRS) of FPCA.

The units forming the FSS are two square metallic patches with different sizes printed on each side of the F4B dielectric substrate as in Fig. 3(a). All the geometry parameters are marked in Fig. 2. As an example, here θ is assumed to be zero, and the optimized sizes are as follows: $P = 8$ mm, $L_1 = 4$ mm, $L_2 = 5.6$ mm, $L_3 = 4$ mm, $L_4 = 1.6$ mm. Fig. 2(d) bottom view shows $W_1 = 7.8$ mm, $W_2 = 7.8$ mm, $W_3 = 7$ mm, $W_4 = 5.8$ mm. Fig. 3(b) shows that the unit cell is simulated by applying Floquet ports and Master/Slaver boundary conditions. And integration lines are also defined.

For RCS reduction surface, Fig. 4 shows the reflection coefficients (S_{11}) of the units. As shown in Fig. 4(a), the reflection magnitudes of FSSs are all above 0.65 from 8.76 to 11.44 GHz. Fig. 4(b) shows that the reflection phase differences among adjacent FSSs are nearly 90° in turn, which indicates that the reflected waves will be cancelled with each other. Therefore, a wideband RCS reduction can be achieved [17].

For PRS, Fig. 5 shows the reflection coefficients (S_{22}) of the FSSs. The reflection magnitudes of the unit cells decrease from inner to outer regions on the substrate, which indicate that FSS units own

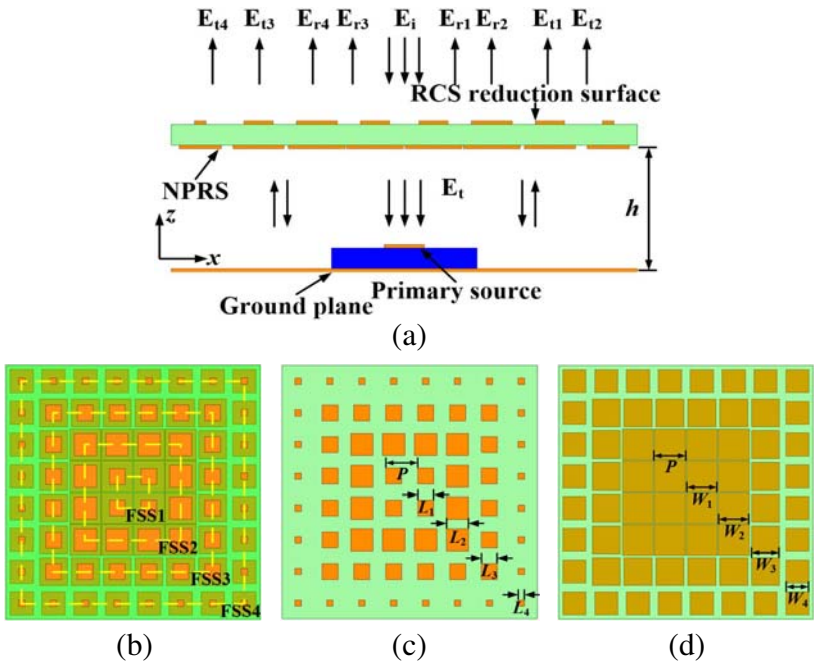

Figure 2. (a) The schematic diagram of the superstrate. (b) The superstrate consisted of four kinds of FSS units. (c) Top view. (d) Bottom view.

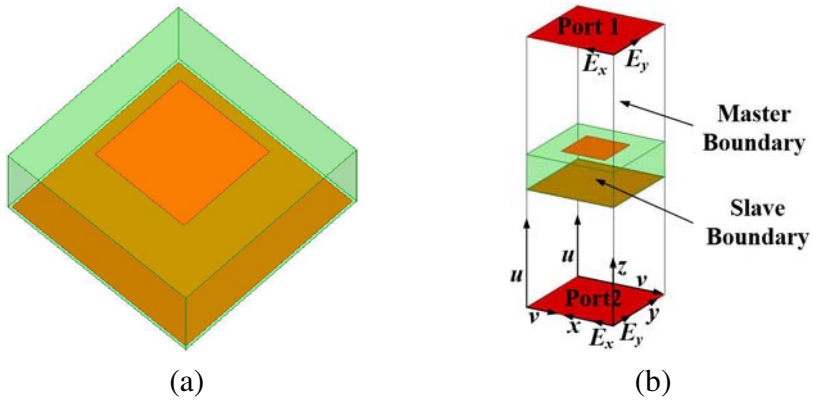

Figure 3. (a) Geometry of the unit. (b) Simulation Floquet ports model of the unit.

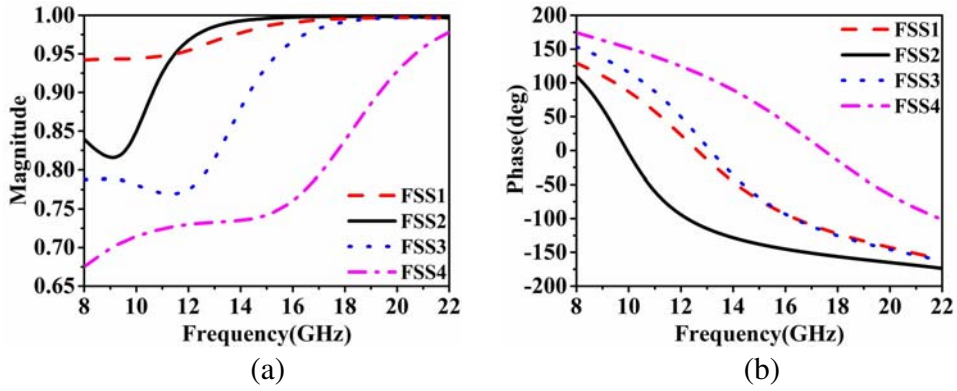

Figure 4. Reflection coefficients (S_{11}) of FSS units. (a) Magnitude. (b) Phase.

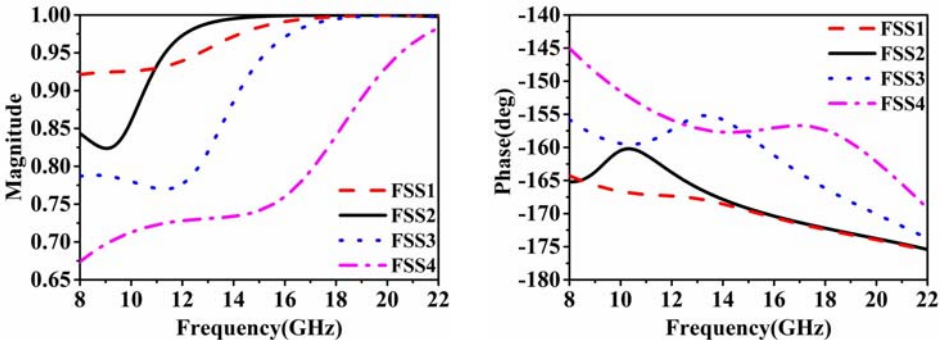

Figure 5. Reflection coefficients (S_{22}) of FSS units. (a) Magnitude. (b) Phase.

negative transverse-reflection magnitude gradient properties. In the meantime, FSS2 and FSS3 possess positive phase gradient properties as shown in Fig. 5(b). As a result, the wideband gain enhancement can be obtained [10, 12].

2.3. Antenna Performance

The geometry of the proposed F-P antenna is given in Fig. 6. The double-sided printed dielectric superstrate with the overall dimension of 64 mm × 64 mm is placed at a height h above a metallic ground plane, and the optimized $h = 18$ mm. The primary source patch antenna is placed at the center of the ground plane to excite the F-P cavity. The primary source patch antenna with the dimension of 5.5 mm×8.4 mm is printed on an F4B substrate with thickness of 3 mm and lateral size of 20 mm×20 mm. The operation frequency bandwidth is from 8.92 to 12.4 GHz, and the center frequency is 10 GHz.

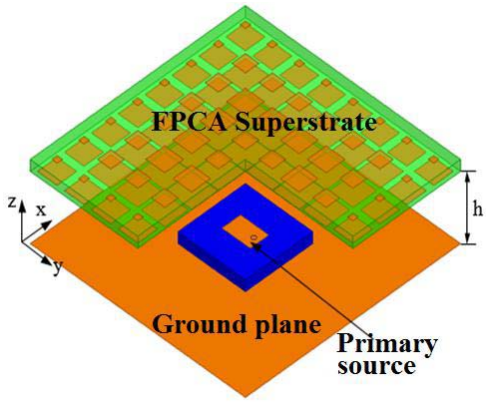

Figure 6. Geometry of the proposed antenna.

Figure 7 shows the electric field of the primary antenna and the FPCA at 9.3 GHz, respectively. The spherical wave of primary antenna is transformed to quasi-plane wave for the antenna loaded with the superstrate. Furthermore, the electric field of the FPCA is almost uniform throughout the cavity due to the application of negative transverse-reflection magnitude gradient reflection magnitudes.

Figure 8 shows the realized gain and monostatic RCS of FPCA and the primary source antenna without superstrate. The gain is above 13.22 dBi in the frequency range from 8.76 to 11.44 GHz (3 dB gain bandwidth 26.53%), and the maximum gain is 16.22 dBi at 9.3 GHz, which is 12.2 dBi larger than that of the primary source antenna. The 3 dB gain bandwidth of the FPCA is 26.53%. The efficiency of the FPCA is also shown. It remains greater than 86% from 8.92 to 12.4 GHz. The proposed antenna can realize RCS reduction from 8.2 GHz to 18.5 GHz, and the maximum RCS reduction value is 31.6 dB at 15 GHz.

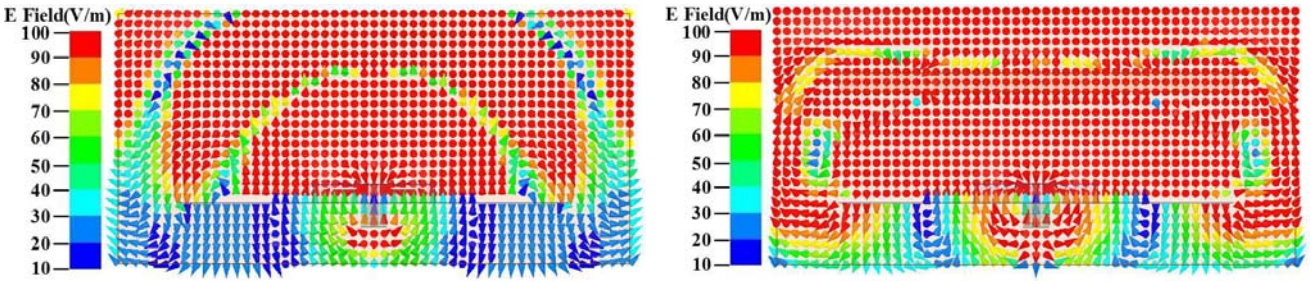

Figure 7. Electric field distributions on the cross section of the antennas at 9.3 GHz. (a) Primary antenna. (b) FPCA.

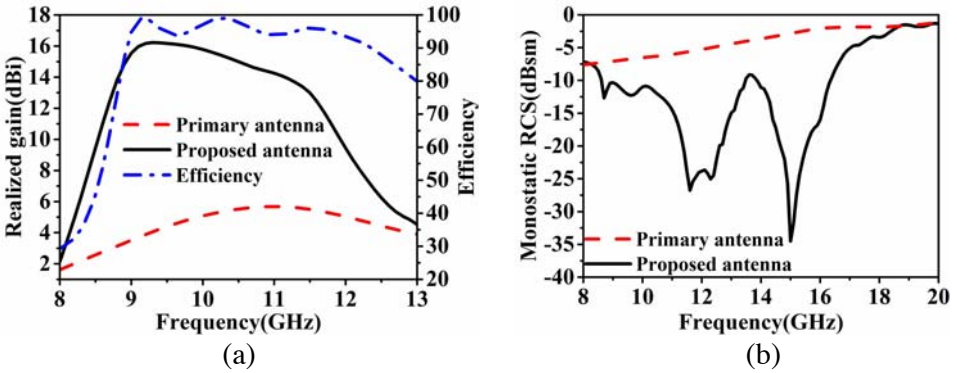

Figure 8. (a) Realized gain of the primary source antenna and the FPCA. Efficiency of the FPCA is also shown. (b) Monostatic RCS of the proposed antenna compared with the primary antenna.

3. EXPERIMENTAL RESULTS

The designed FPCA is fabricated and measured to verify its wide band, high gain, and high aperture efficiency performance. The prototype of the whole structure is in Fig. 9(a). Four Nylon spacers are used to support the cavity. The measurement environment is shown in Fig. 9(b). The measurements of the fabricated antenna are completed in a microwave anechoic chamber. Fig. 10 shows the simulated and measured S_{11} and realized gain of patch and proposed antennas. It can be observed that simulations agree well with measurements. As shown in Fig. 10(a), the measured $S_{11} < -10$ dB bandwidth ranges from 8.9 to 12.4 GHz (32.86%). Fig. 10(b) shows that the proposed antenna has a measured 3 dB gain

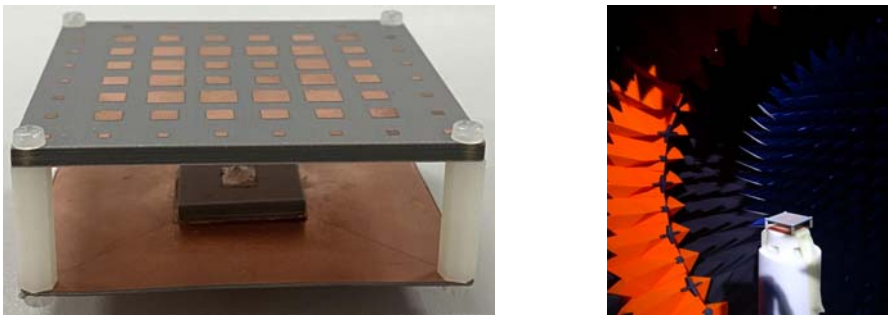

Figure 9. (a) Photograph of the prototype. (b) Measurement circumstance.

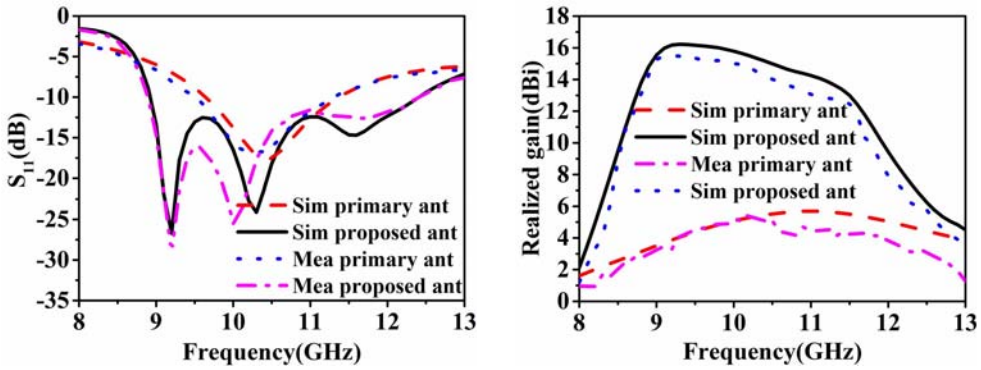

Figure 10. Simulated and measured results of patch and proposed antennas. (a) S_{11}. (b) Realized gain.

bandwidth of 26.9%, extending from 8.75 to 11.47 GHz with a peak gain of 15.5 dBi at 9.2 GHz. The aperture efficiency is 73.3%. The simulated and measured radiation patterns in the E- and H-planes at 9 GHz, 10 GHz, and 11 GHz are shown in Fig. 11. It can be observed that the main beam of the proposed antenna is highly directive toward broadside throughout the band. However, the patterns in the E-planes are asymmetric, because the unsymmetrical field is radiated by the primary feed inside the cavity. The average sidelobe levels (SLLs) remain a low level at 9 GHz and 10 GHz, but they increase to -4 dB at 11 GHz. This phenomenon is common in broadband resonant cavity antennas that the SLL in the E-plane usually increases to -5 dB. Meanwhile, the cross-polarization levels at the broadside direction are all less than -35 dB in the E-plane. In the H-plane, the SLL remains under -10 dB and the cross-polarization levels are under -15 dB from 9 GHz to 11 GHz.

The measured and simulated monostatic RCSs of the FPCA under normal incidence are shown in

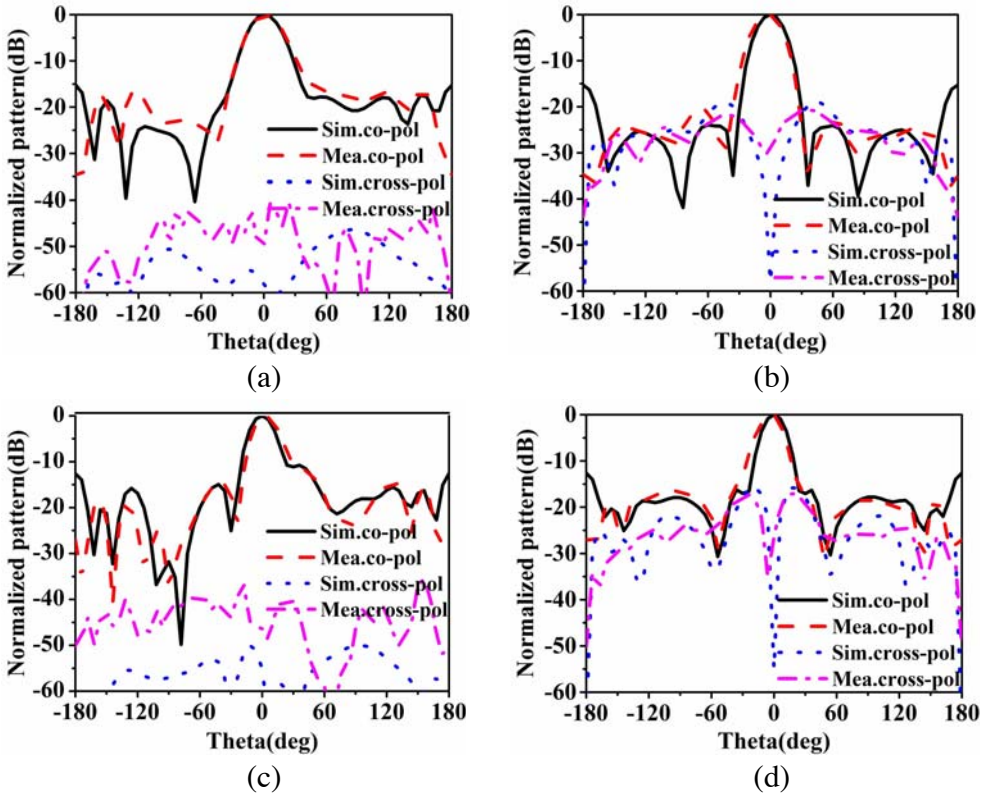

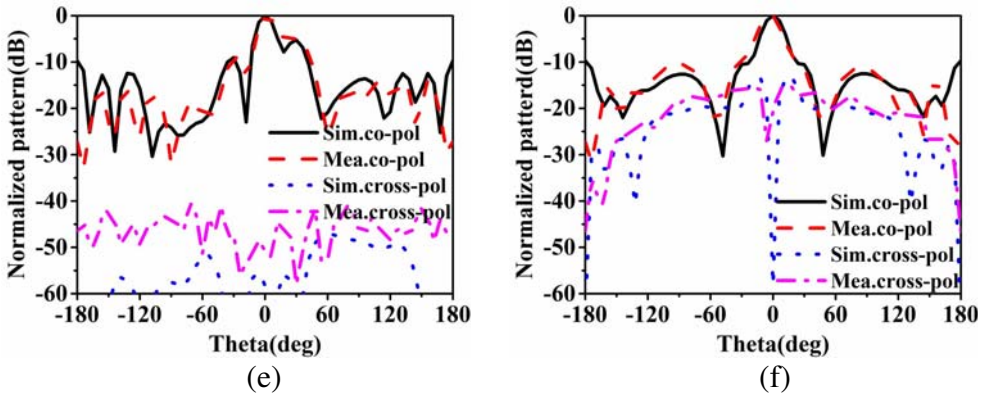

Figure 11. Radiation patterns of the proposed antenna. (a) E-plane and (b) H-plane at 9 GHz, (c) E-plane and (d) H-plane at 10 GHz, (e) E-plane and (f) H-plane at 11 GHz.

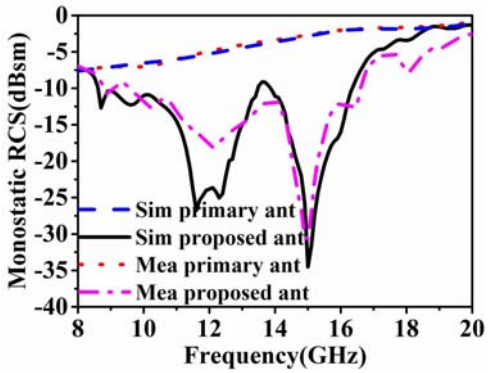

Figure 12. Simulated and measured RCS reduction of the proposed antenna.

Table 1. Comparison of the proposed antenna with the similar designs in reference.

References	Impedance BW (%)	3-dB Gain BW (%)	Aperture Efficiency (%)	Peak Gain (dBi)	Area (λ_0^2)	RCS Reduction BW (%)
[20]	3.5	2	40.2	18.4	13.69	72
[21]	11.08	N/A	20.5	12.3	6.59	88.9
[5]	2.1	4.8	55.5	19.8	13.5	40
[22]	6.9	3.7	31.4	13.2	5.29	80
[13]	18.6	16.58	18.8	11.9	4.84	76.92
This work	32.86	26.9	73.3	15.5	3.85	83.7

Fig. 12. It can be observed that considerable RCS reduction is obtained from 8.2 to 20 GHz with a relative bandwidth of 83.7%, covering the in-band and out-band. A comparison with some published FPCAs with RCS reduction is made in Table 1, highlighting the functionality of the proposed structure. It is obvious that the proposed antenna provides wider 3-dB gain bandwidth, impedance bandwidth, smaller size, and high aperture efficiency. In addition, RCS reduction covers the operating band of the FPCA, corresponding to an RCS reduction bandwidth of 83.7%.

4. CONCLUSION

A broadband high-gain, high aperture efficiency, and low RCS FPCA is presented. The high aperture efficiency and wideband are obtained by utilizing the PRS with the properties of positive reflection phase gradient and negative transverse-reflection magnitude gradient. The 10-dB impedance bandwidth is 32.86%, 3-dB gain bandwidth 26.9%, the aperture efficiency 73.3%, and the measured peak gain 15.5 dBi. The wideband RCS reduction is realized by designing the phase differences 90° in turn among four frequency-selective surfaces. Wideband RCS reduction from 8.2 to 20 GHz (83.7%) is achieved. The proposed FPCA has the following performances simultaneously: wideband $|S_{11}|$ bandwidth, high gain, high aperture efficiency, and low RCS. The proposed antenna shows excellent radiation performances and scattering performances, which has potential application in the stealth technology.

ACKNOWLEDGMENT

This work was supported by the Key Project of Natural Science Foundation of Guangdong Province of China under Grant 2018B030311013, the National Natural Science Foundation of China under Grant 61071056.

REFERENCES

1. Feresidis, A. P., G. Goussetis, S. Wang, and J. C. Vardaxoglou, "Artificial magnetic conductor surfaces and their application to low-profile high-gain planar antennas," *IEEE Trans. Antennas Propag.*, Vol. 53, No. 1, 209–215, Jan. 2005.
2. Wiesbeck, W. and E. Heidrich, "Influence of antennas on the radarcross section of camouflaged aircraft," *Proc. Int. Conf. Radar*, 122–125, 1992.
3. Pan, W., C. Huang, P. Chen, X. Ma, C. Hu, and X. Luo, "A low-RCS and high-gain partially reflecting surface antenna," *IEEE Trans. Antennas Propag.*, Vol. 62, No. 2, 945–949, Feb. 2014.
4. Jiang, H., Z. Xue, W. Li, W. Ren, and M. Cao, "Low-RCS high-gain partially reflecting surface antenna with metamaterial ground plane," *IEEE Trans. Antennas Propag.*, Vol. 64, No. 9, 4127–4132, Sep. 2016.
5. Zhang, L., et al., "Realization of low scattering for a high-gain Fabry-Pèrot antenna using coding metasurface," *IEEE Trans. Antennas Propag.*, Vol. 65, No. 7, 3374–3383, Jul. 2017.
6. Hashmi, R. M., B. A. Zeb, and K. P. Esselle, "Wideband high-gain EBG resonator antennas with small footprints and all-dielectric super structures," *IEEE Trans. Antennas Propag.*, Vol. 62, No. 6, 2970–2977, Jun. 2014.
7. Hashmi, R. M. and K. P. Esselle, "A class of extremely wideband resonant cavity antennas with large directivity-bandwidth products," *IEEE Trans. Antennas Propag.*, Vol. 64, No. 2, 830–835, Feb. 2016.
8. Lalbakhsh, A., M. U. Afzal, K. P. Esselle, and S. L. Smith, "A high-gain wideband EBG resonator antenna for 60 GHz unlicenced frequency band," *Proc. 12th Eur. Conf. Antennas Propag.*, 1–3, London, U.K., Apr. 2018.
9. Afzal, M. U. and K. P. Esselle, "A low-profile printed planar phase correcting surface to improve directive radiation characteristics of electromagnetic band gap resonator antennas," *IEEE Trans. Antennas Propag.*, Vol. 64, No. 1, 276–280, Jan. 2016.
10. Lalbakhsh, A., M. U. Afzal, K. P. Esselle, S. L. Smith, and B. A. Zeb, "Single-dielectric wideband partially reflecting surface with variable reflection components for realization of a compact high-gain resonant cavity antenna," *IEEE Trans. Antennas Propag.*, Vol. 67, No. 3, 1916–1921, Mar. 2019.
11. Wang, N., Q. Liu, C. Wu, L. Talbi, Q. Zeng, and J. Xu, "Wideband Fabry-Perot resonator antenna with two complementary FSS layers," *IEEE Trans. Antennas Propag.*, Vol. 62, No. 5, 2463–2471, May 2014.

12. Ge, Y., K. P. Esselle, and T. S. Bird, "The use of simple thin partially reflective surfaces with positive reflection phase gradients to design wideband, low-profile EBG resonator antennas," *IEEE Trans. Antennas Propag.*, Vol. 60, No. 2, 743–750, Feb. 2012.
13. Zheng, Y., J. Gao, Y. Zhou, X. Cao, H. Yang, and S. Li, "Wideband gain enhancement and RCS reduction of Fabry-Perot resonator antenna with Chessboard arranged metamaterial superstrate," *IEEE Trans. Antennas Propag.*, Vol. 66, No. 2, 590–599, Feb. 2018.
14. Zhou, L., X. Chen, and X. Duan, "Fabry-Pérot resonator antenna with high aperture efficiency using a double-layer nonuniform superstrate," *IEEE Trans. Antennas Propag.*, Vol. 66, No. 4, 2061–2066, Apr. 2018.
15. Galarregui, J. C. I., A. T. Pereda, J. L. M. de Falcón, I. Ederra, R. Gonzalo, and P. de Maagt, "Broadband radar cross-section reduction using AMC technology," *IEEE Trans. Antennas Propag.*, Vol. 61, No. 12, 6136–6143, Dec. 2013.
16. Paquay, M., J.-C. Iriarte, I. Ederra, R. Gonzalo, and P. de Maagt, "Thin AMC structure for radar cross-section reduction," *IEEE Trans. Antennas Propag.*, Vol. 55, No. 12, 3630–3638, Dec. 2007.
17. Jia, Y., Y. Liu, S. Gong, W. Zhang, and G. Liao, "A low-RCS and high-gain circularly polarized antenna with a low profile," *IEEE Antennas Wireless Propag. Lett.*, Vol. 16, 2477–2480, 2017.
18. Lian, R., Z. Tang, and Y. Yin, "Design of a broadband polarization reconfigurable Fabry-Perot resonator antenna," *IEEE Antennas Wirel. Propag. Lett.*, Vol. 17, No. 1, 122–125, Jan. 2018.
19. Trentini, G. V., "Partially reflecting sheet arrays," *IRE Trans. Antennas Propag.*, Vol. 4, No. 4, 666–671, Oct. 1956.
20. Jiang, H., Z. Xue, W. Li, W. Ren, and M. Cao, "Low-RCS high-gain partially reflecting surface antenna with metamaterial ground plane," *IEEE Trans. Antennas Propag.*, Vol. 64, No. 9, 4127–4132, Sep. 2016.
21. Mu, J., H. Wang, H.-Q. Wang, and Y. Huang, "Low-RCS and gain enhancement design of a novel partially reflecting and absorbing surface antenna," *IEEE Antennas Wireless Propag. Lett.*, Vol. 16, 1903–1906, 2017.
22. Ren, J., W. Jiang, K. Zhang, and S. Gong, "A high-gain circularly polarized Fabry-Perot antenna with wideband low-RCS property," *IEEE Antennas Wireless Propag. Lett.*, Vol. 17, No. 5, 853–856, May 2018.